scientific reports

Check for updates

OPEN

Computational exploration of Eucommia ulmoides flavonoids as potential RANKL inhibitors via molecular docking and dynamics simulations

Xiaofei Zhang[1,5], Lixia Zhang[2,5], Dan Li[1], Qi Wang[3], Libin Wang[1], Ziqi Zheng[4] & Yun Xie[1]✉

Osteoporosis, characterized by excessive osteoclast activation, is mediated through the RANKL/RANK/OPG signaling axis. While flavonoids from *Eucommia ulmoides* (EU) have demonstrated anti-osteoclastogenic activity, their atomic-level mechanisms remain elusive. Here, we investigated six EU-derived flavonoids (cyrtominetin, quercetin, syringetin, genistein, ombuin, and kaempferol) targeting RANKL using integrated computational approaches. Molecular docking revealed strong binding affinities (Total_Score > 4.0) for all compounds, with cyrtominetin exhibiting the highest affinity (-50.205 kJ/mol via MM-PBSA), primarily through hydrogen bonds with Gly178, His180, Lys181, and Asn295. Moreover, most flavonoids interacted with RANKL by forming strong hydrogen bonds with Gly178 and Asn295, exhibiting higher binding affinity that was identified as essential for the activity. All-atom molecular dynamics simulations (100 ns) confirmed complex stability, demonstrating: low RMSD fluctuations (< 4.0 Å) and compact Rg values (16.0–17.0 Å). Notably, binding free energy decomposition identified both electrostatic and van der Waals contributions as critical for stabilization. These results identify cyrtominetin as a promising lead compound for RANKL inhibition, providing structural insights for designing flavonoid-based therapeutics against osteoporosis.

Keywords Osteoporosis, Flavonoids, RANKL, Molecular docking, Molecular dynamics

Osteoporosis, the most prevalent metabolic bone disorder, is characterized by low bone density, decreased bone mass and increased bone fragility[1]. With a global prevalence exceeding 100 million cases, osteoporosis has been designated by the World Health Organization (WHO) as a major public health challenge of international concern[2]. Bone mass homeostasis is maintained through a dynamic biological process termed bone remodeling, which is regulated by the balanced interplay between osteoclast-mediated bone resorption and osteoblast-driven bone formation[3]. Accumulating evidence indicates that the dysregulation of the equilibrium between bone resorption and bone formation results in osteoporosis. In particular, the overactivation of osteoclasts has been identified as the principal determinant of excessive bone resorption and the consequent decline in bone mineral density[4]. Therefore, targeted inhibition of osteoclast-mediated bone resorption to restore physiological bone remodeling equilibrium has been established as a fundamental treatment strategy in osteoporosis therapeutics[5].

The differentiation and maturation of osteoclasts is a complex and delicate multilevel regulatory process wherein the receptor activator of nuclear factor-κB ligand (RANKL) functions as the principal signaling molecule governing this pathway[6]. Specifically, the binding of RANKL to the receptor activator of nuclear factor-κB (RANK) induces tumor necrosis factor receptor-associated factor 6 (TRAF6) recruitment, which sequentially activates signaling factors nuclear factor kappa-B (NF-κB) and mitogen-activated protein kinases (MAPKs), including p38, c-Jun N-terminal kinase (JNK) and extracellular signal-regulated kinase (ERK)[7,8]. In parallel, the RANKL-RANK interaction activates the AKT signaling pathway by recruiting c-Src[9,10]. Subsequently, activation of these signaling molecules upregulates the expression of nuclear factor of activated

[1]Department of Laboratory Medicine, Northwest Womens and Childrens Hospital, 1616 Yanxiang Road, Xi'an 710061, Shaanxi, China. [2]Department of Clinical Laboratory, Shaanxi Provincial Peoples Hospital, Xi'an, China. [3]Department of Clinical Laboratory, Second Affiliated Hospital of Xian Jiaotong University, Xi'an, Shaanxi, China. [4]College of Life Sciences, Northwest University, 229 North Taibai Road, Xi'an, Shaanxi 710069, People's Republic of China. [5]Xiaofei Zhang and Lixia Zhang contributed equally to this work. ✉email: xieyunhero@sina.com

T-cell c1 (NFATc1) and c-Fos, which can directly regulate osteoclast differentiation and osteoclast-specific gene expression[11]. In addition, osteoprotegerin (OPG), a natural antagonist of RANKL, inhibits osteoclastogenesis by preventing RANKL/RANK interaction[12]. Based on the above analysis, targeting the RANKL/RANK/OPG axis of osteoclast differentiation signaling pathway, especially directly Inhibiting RANKL-RANK interaction, may offer a promising strategy for developing novel therapeutic approaches against osteoporosis[13].

Currently, many researchers are actively investigating potential drugs to antagonize or inhibit RANKL. Unfortunately, most identified compounds exhibit limitations that restrict their clinical application[14]. Denosumab, a monoclonal antibody targeting RANKL, was developed for osteoporosis treatment[15]. As the first FDA-approved RANKL inhibitor, its application remains limited by high costs[16]. Furthermore, recombinant protein-based therapeutics, including Fc-OPG fusion proteins and other anti-RANKL antibodies, have been developed as therapeutic agents for osteoporosis[17,18]. However, the clinical applications of these macromolecular drugs are hindered by some shortcomings, such as low stability, poor bioavailability, high cost, and difficulties in administration[19].

Natural product libraries are being increasingly explored to find more specific and safer agents against RANKL. For example, it has been found that ellagic acid, niloticin and epigallocatechin-3-gallate can directly block RANKL-RANK interaction to inhibit RANKL-induced osteoclast differentiation signaling pathway[20,21]. In fact, numerous flavonoid compounds exhibit inhibitory effects on both RANKL-induced osteoclast differentiation and bone resorption[22–24]. Such as, quercetin can affect NF-kB, AP-1 and NFATc1 in RANKL/RANK/OPG system to inhibit osteoclast differentiation[25]. Kaempferol can inhibit RANKL-mediated ERK, JNK and p38 phosphorylation and the expression of c-Fos and NFATc1[26,27]. Genistein directly inhibits osteoclastic differentiation through inhibiting the expression of two transcription factors c-Fos and NFATc1 induced by NF-kB up regulation[28]. Syringetin has been identified as an inhibitor targeting osteoclast differentiation[29]. Moreover, KEGG pathway revealed that the flavonoids in *Eucommia ulmoides* (EU) directly regulate the osteoclast differentiation signaling pathways to treat osteoporosis[30]. Given the demonstrated ability of flavonoids to suppress RANKL-induced activation of AKT, MAPK, and NF-κB signaling pathways while regulating osteoclast differentiation pathways, we speculated that these compounds could disrupt RANKL–RANK interaction through competitive binding to RANKL, thereby inhibiting osteoclastogenesis.

Here, we described the ability of flavonoids to bind RANKL using molecular docking and molecular dynamics simulations. Molecular simulations can provide detailed information at the atomic level, including quantitative and thermodynamic descriptions of receptor-ligand interactions with high resolution, which are difficult to obtain through experimental approaches[31]. The six flavonoids previously reported in the EU, including quercetin, kaempferol, cyrtominetin, syringetin, genistein and ombuin, were specifically selected for the present study[30]. We believe that the results of molecular simulations can provide deeper insights into understanding the underlying mechanisms of flavonoids to inhibit RANKL-induced osteoclastogenesis at the atomic level, and facilitate the development of new medications for osteoporosis.

Results

Preparation of ligand and protein for docking

The details of six flavonoids with positive ADMET properties in this study were shown in Table 1. The radar plot demonstrates that all physicochemical properties fall within the desirable range. PROCHECK was used to assess the stereochemical quality of the protein structure by analyzing residue-by-residue geometry and overall structure geometry. Ramachandran plot analysis revealed that 89.1% of residues fall in the most favorable regions, 9.5% in additional allowed regions, 1.5% in generously allowed regions, and none in disallowed regions (Fig. 1).

Binding site prediction

3URF includes two parts, RANKL and its decoy receptor OPG. The binding interface of RANKL/OPG is composed of two binding sites (Fig. 2)[32]. The binding site I, composed of relatively small and separate contact patches in both RANKL and OPG, is located on the OPG"50 s loop"(His47-Leu65) and nearly parallel to the RANKL along the groove. Whereas at the binding site II, the OPG “90 s loop” (Arg90 -Leu98) is deeply within the groove. Compared with separate interactions at the binding site I, more interactions at the binding site II are concentrated around the tip of OPG 90 s loop. The binding site II forms a hydrophilic interaction network with RANKL residues by using Glu95 of the OPG"90 s loop", which is more important than the binding site I in RANKL/OPG binding. At the same time, this position is also the main binding determinant of RANKL/RANK interaction. Additionally, after binding with RANKL active site, Glu93 and Ile94 residues were observed to form hydrophobic and van der Waals (vdW) interactions with hydrophobic residues around RANKL. Three amino acids, Glu93, Ile94, and Glu95, from the OPG probe deeply into the concave surface of RANKL, defining the main binding pocket for small molecular inhibitors targeting RANKL/RANK interaction. Residues within a distance of 6 Å around the residues Glu93, Ile94, and Glu95 of OPG were defined as the binding pocket for molecular docking[33].

Molecular interaction

In molecular docking, ligands bind to amino acid residues within the active site, participating in the process of conformational changes and energy complementation. The binding sites and binding score values can intuitively reflect the interaction and stability of the docking model. The docking results showed that all flavonoids exhibited notable interactions and docking scores were greater than 4, indicating that the binding between flavonoids and RANKL was relatively stable. Among picked molecules, cyrtominetin and quercetin displayed the best binding affinities compared to other molecules with Total_Score of 6.5143 and 5.0316 respectively. The control group had a Total_Score of 6.3254. Interestingly, cyrtominetin achieved a superior binding than control group suggesting

PubChem CID	Name	Molecular formula	2D Structure	Physicochemical property
125,309	Cyrtominetin	$C_{17}H_{16}O_6$	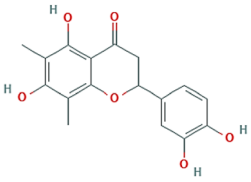	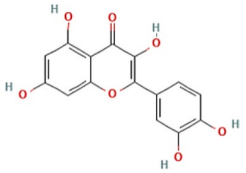
5,280,343	Quercetin	$C_{15}H_{10}O_7$	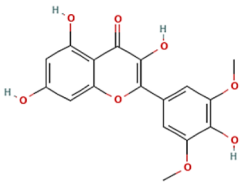	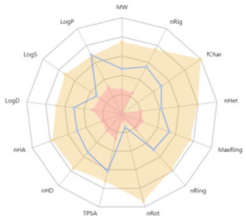
5,281,953	Syringetin	$C_{17}H_{14}O_8$	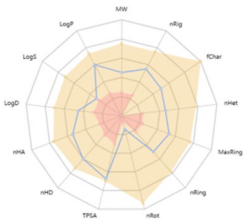	
5,280,961	Genistein	$C_{15}H_{10}O_5$	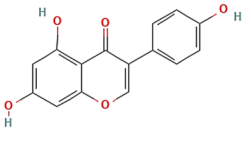	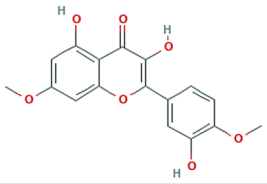
5,320,287	Ombuin	$C_{17}H_{14}O_7$	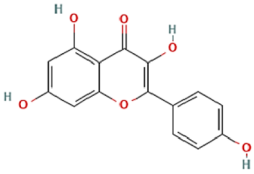	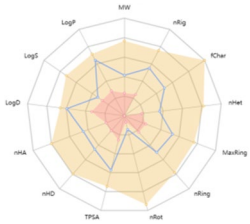
5,280,863	Kaempferol	$C_{15}H_{10}O_6$	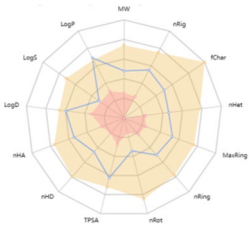	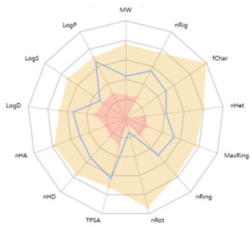

Table 1. The structural information and physicochemical properties of flavonoids. The range of yellow, red, and blue represent upper limit, lower limit, and compound properties, respectively.

that it has a promising affinity and intrinsic activity toward the RANKL. The binding modes of RANKL with the 6 flavonoids were shown in Fig. 3.

After exploring the molecular interactions, it was perceived that cyrtominetin manifested hydrogen bonds with residues Gly178, His180, Lys181, and Asn295. One amide-Pi stacked with residues Ser179, one Pi-alkyl (His180), and one alkyl interaction (Met239). It also formed vdW interaction with residues Val182, Thr233, Gln237, Tyr241, Ser294, and Pro296. In the case of quercetin, residue Gly178, Lys181, Gln237, and Asn295 formed hydrogen bonds. Residues Ser179 interacted via Pi-lone pair interactions. Residues His180, Met239, Tyr241, Ser294 and Pro296 formed vdW interactions. In molecule syringetin, residues Gly178, Lys181, Gln237, and Asn295 formed hydrogen bonds. Several residues formed other interactions like Ser179 (Pi-lone pair), Tyr241 (Pi-alkyl), Met239 (Alkyl), and residues His180, Lys257, Ser294 and Pro296 showed vdW interactions. In genistein, hydrogen bonds were formed by residues Gly178, Gln237, Asn295, and C-H bond by Ser294, Leu236. Residues Ser179 also formed amide-Pi stacked. Residues Lys181, Val182, Tyr235, Thr261, Pro296 and Ser294 showed vdW interactions. In the case of ombuin, hydrogen bonds were formed by residues Gly178, Thr233,

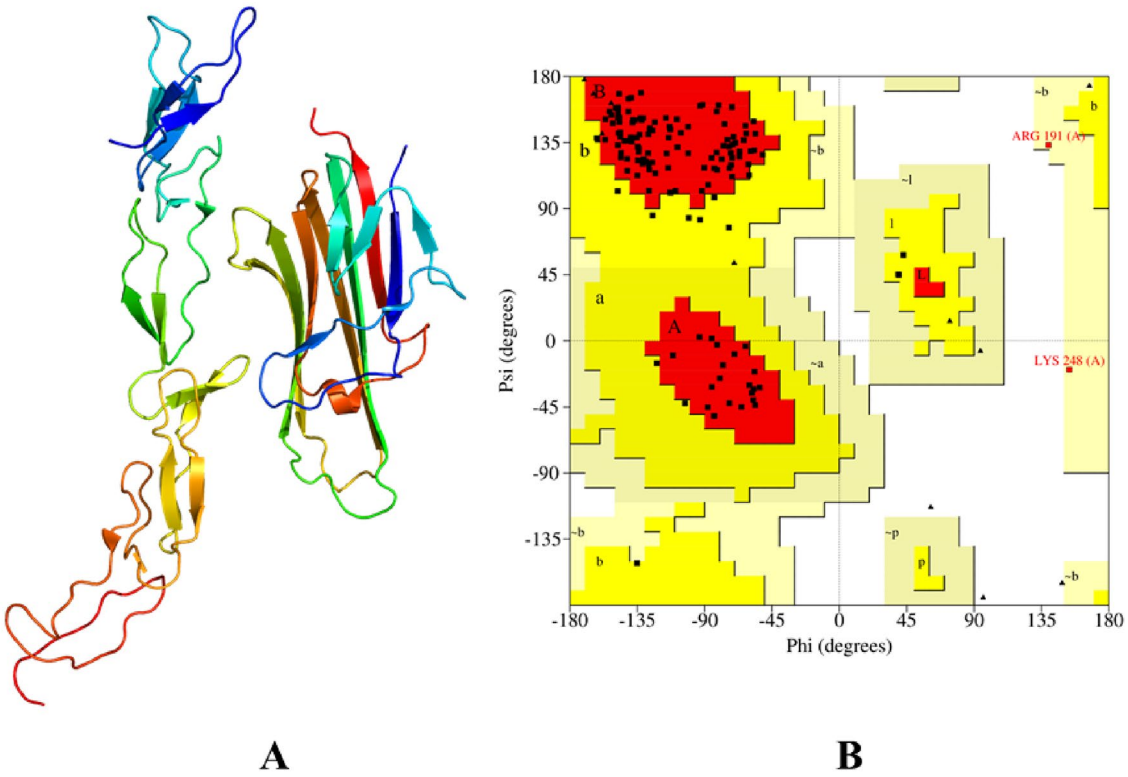

Fig. 1. (**A**) Overall structure of RANKL/OPG complex. (**B**) The Ramachandran plot of RANKL. Red, yellow, light yellow, and white are the most favorable, additional allowed, generously allowed, and disallowed regions in conformation, respectively.

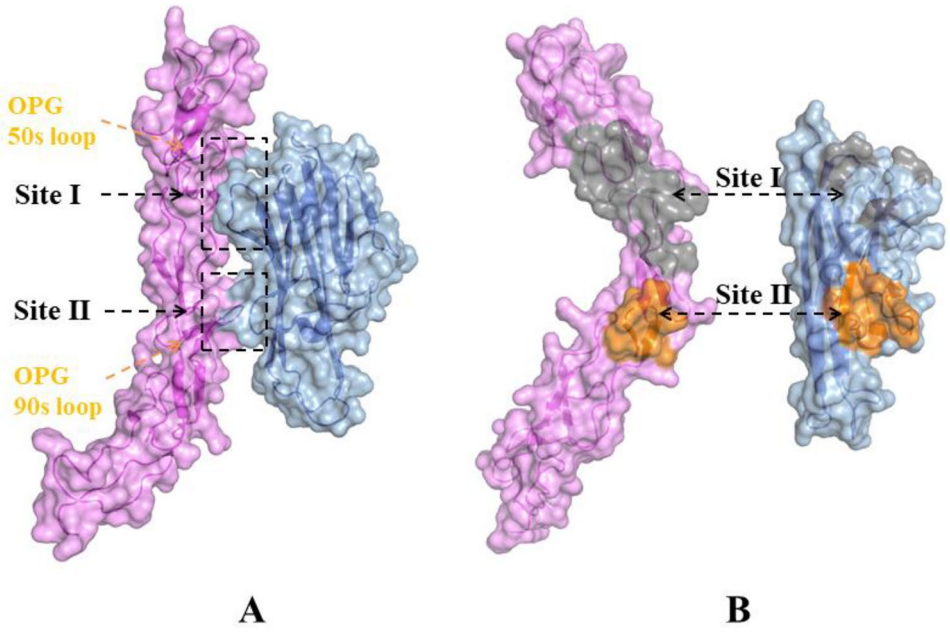

Fig. 2. Overall view of RANKL/OPG binding interface. (**A**) Sites I and II in the binding interface. The OPG is shown in surface colored with violet. The RANKL is colored with blue. (**B**) An open-book view of the contact residues in binding sites I and II. The contact residues in binding sites I and II are colored with grey and orange, respectively.

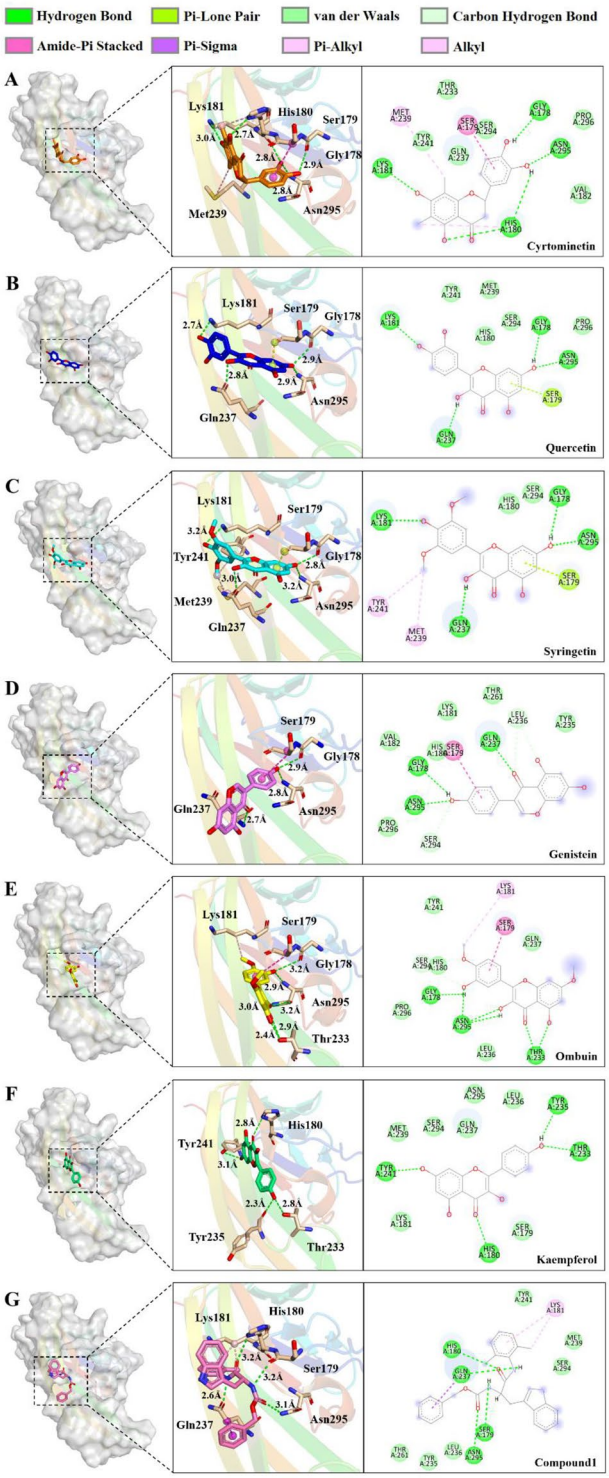

Fig. 3. Binding mode of flavonoids in the active site of RANKL. (**A**) Cyrtominetin (orange), (**B**) Quercetin (blue), (**C**) Syringetin (cyan), (**D**) Genistein (purple), (**E**) Ombuin (yellow), (**F**) Kaempferol (green), and (**G**) control group (pink). Protein residues are shown in pale gold sticks.

Asn295, and C-H bond by His180. Residues also formed other interactions, including one amide-Pi stacked (Ser179), and alkyl (Lys181). Residues Tyr235, Leu236, Gln237, Tyr241, Ser294, and Pro296 displayed vdW interactions. Kaempferol exhibited hydrogen bonds with residue His180, Thr233, Tyr235, and Tyr241. It also formed vdW interaction with residues Ser179, Lys181, Leu236, Gln237, Met239, Ser294, and Asn295. In control group, hydrogen bonds were formed by residues Ser179, His180, Gln237, Asn295, and C-H bond by Ser179.

Residues also formed other interactions, including one Pi-sigma (Gln237), Pi-alkyl (Lys181), and alkyl (Lys181). Residues Tyr235, Leu236, Met239, Tyr241, Thr261 and Ser294 showed vdW interactions.

The binding style contributes a reasonable rationale for the significance of interacting residues in target protein binding. It was observed that the 6 flavonoids share remarkable structural similarities, occupying virtually identical binding pocket. Furthermore, the binding of flavonoids to RANKL was also significantly mediated by the critical residues and conferred the best interactions. These data indicated that residues Gly178, Asn295, Lys181, Gln237, and Ser179 played a more critical role in the binding process.

Molecular dynamics simulations

Molecular dynamics simulation is an efficacious approach for evaluating the stability of protein–ligand complexes identified through docking studies and characterizing their dynamic properties[34]. From the result of docking, the protein–ligand complex having the least binding energy with the best configuration was carried out 100 ns MD simulation.

RMSD analysis

RMSD of backbone C-α atoms was measured using the GROMACS "gmx rmsd" tool to quantify the structural stability of protein–ligand complex. Generally, RMSD is a standard measurement of the structural distance between coordinates, which is used to infer the extent of deviation for a group of atoms relative to their initial structures[35]. The RMSD values express how much the conformations of these groups of atoms have changed to indicate the stability of complexes. A low RMSD (< 2.0 Å) reflects high conformational stability near the initial structure, while moderate (2.0–3.0 Å) and high (> 3.0 Å) values indicate local relaxation (e.g., flexible loops/sidechains) and significant structural changes respectively, the latter requiring complementary metrics (e.g., RMSF) to assess potential functional transitions. As shown in Fig. 4, all complexes reached RMSD equilibrium within 15–30 ns, indicating that the simulated systems departed from initial artificial conformations and attained thermodynamic equilibrium. The post-equilibrium RMSD fluctuation amplitudes reflect intrinsic protein flexibility rather than structural instability, with all variations remaining within acceptable limits (overall RMSD < 3.00 Å), demonstrating the stability of the conformational ensemble.

The cyrtominetin-bound protein started from C-alpha RMSD (RMSD-Cα) 1.07 Å, gradually increasing until it converged at around 15 ns. After this, the protein adopted an equilibrium plateau showing minimal fluctuations around its average until the end of the MD run with an average deviation of 2.86 Å. This behavior is a typical MD simulation run, in which the protein begins to relax after removing all constraints until reaching its equilibration state, where RMSD-Cα trajectories tends to be stable indicating the stability of the protein. In the case of quercetin-bound protein, the backbone RMSD gradually increased until convergence at around 30 ns where RMSD tends to be stable until reaching 50 ns, in which RMSD decreased then rose again. The final convergence around an average RMSD (2.66 Å) started from 60 ns until the end of MD simulation at 100 ns. The simulation of syringetin-bound protein performed well, in which it gradually reached dynamic equilibration at around 25 ns, and the average RMSD was 2.33 Å with stable fluctuations until 100 ns. The RMSD-Cα trajectories of genistein-bound protein had a low average value (2.15 Å) and lesser fluctuations, indicating its stability. With regard to ombuin and kaempferol, the proteins started at lower RMSD-Cα values (0.71 and 0.78 Å, respectively), and proteins depicted delayed convergences after 30 ns from the start of the MD simulation runs. Following convergence, both proteins were dynamically balanced, showing their RMSD-Cα trajectories being maintained around their respective average deviations (1.17 Å and 2.89 Å, respectively). The

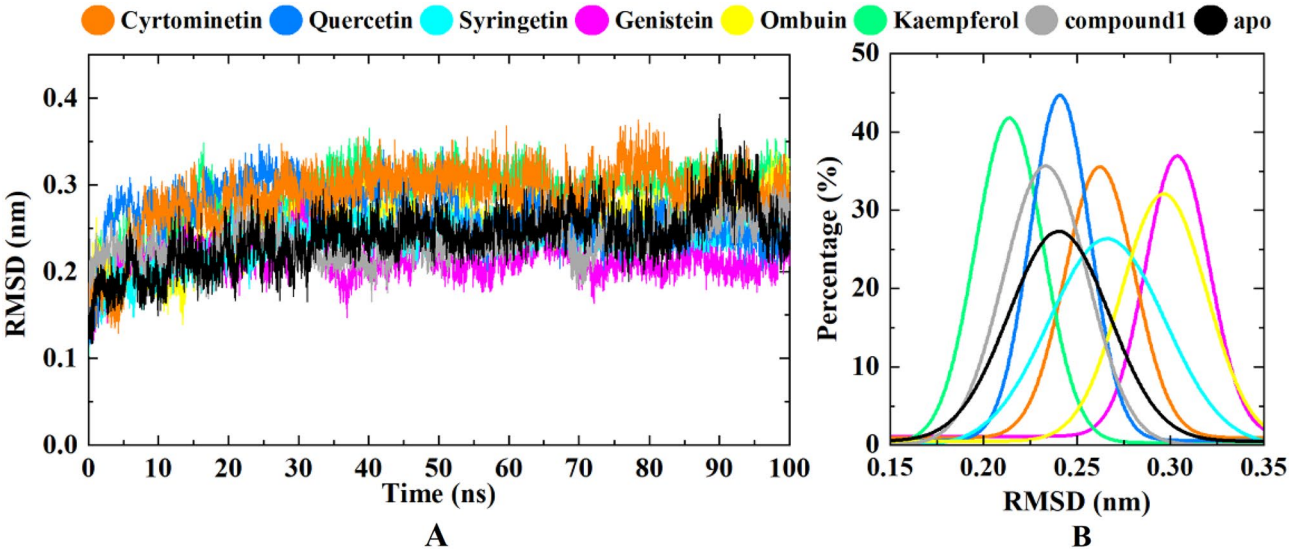

Fig. 4. Time evolution RMSD trajectories of the RANKL-flavonoids complexes over 100 ns all-atom MD simulation. (**A**) The RMSD of backbone Cα-atoms. (**B**) The relative frequency distribution of RMSD.

RANKL apo state was initially stable and maintained structural integrity during most of the simulation time. However, a rise of the RMSD value was observed for 85–95 ns time and returned to the steady state in the final period (average 2.38 Å), potentially attributable to solvent effects or natural conformational fluctuations. Collectively, the RMSD trajectories demonstrate that all systems maintained stable conformational ensembles throughout the 100 ns simulations. The RMSD-Cα values for all six flavonoid-RANKL complexes remained below 3.0 Å, indicating that ligand binding did not significantly perturb the global protein structure. These stable conformational samplings provide a reliable foundation for subsequent binding free energy calculations.

RMSF analysis

To characterize residue-specific flexibility, we conducted RMSF calculations that measure the positional fluctuations of individual amino acid residues about their mean coordinates throughout the MD trajectories, thereby elucidating local protein dynamic properties. The individual backbone RMSF was calculated using the GROMACS "gmx rmsf" command line to perceive structural stability and flexibility at local levels. In addition, it can also be used to identify the flexible residues in the protein, so that we can explore the conformational flexibility of the protein structure[36].

As depicted in Fig. 5, all systems showed almost similar patterns. In the case of RANKL apo state, we observed the highest fluctuations in loop regions. The loop regions are very flexible elements of protein, and their flexibility is essential to accommodate the ligand at the binding site appropriately. For the residues (178–181, 237–241, and 293–296) at the binding site, the RMSF had smaller values throughout the simulation, further showing the regions of active site residues were quite stable. Compared with the RANKL apo state, the RMSF values of numerous residues in RANKL-flavonoids complexes increased, especially residues in loop regions, indicating that the flexibility of RANKL monomer increased after binding with flavonoids. These observations align with the coupled dynamics theory of protein–ligand systems, where binding stabilizes functional residues (low RMSF) while permitting peripheral flexibility (high RMSF) to maintain biological activity. The flavonoid-induced flexibility increase in RANKL loops may reflect allosteric communication between binding and effector sites. Notably, the low RMSF values (< 3 Å) of active-site residues underscores their thermodynamic favorability for flavonoid recognition, corroborating the stable binding modes inferred from MM/PBSA calculations.

Radius of gyration

Next, we investigated the structural stability of the protein–ligand complex by calculating the Rg, which determines the compactness of the protein structure. The Rg was calculated using the GROMACS"gmx gyrate"script. This parameter provides insight into protein folding and unfolding dynamics upon ligands binding. Higher Rg values explain less compactness (more unfolded) with high conformational entropy while low Rg values show high compactness and more stability in the structure (more folded)[37].

As shown in Fig. 6, all systems of ligand-bound proteins have projected the Rg values between 16 to 17 Å. To some extent, the protein Rg values were comparable among the investigated systems being fluctuated around close averages. In the case of RANKL apo state, the average Rg value was found to be 16.94 Å. The average Rg values of cyrtominetin-bound protein and quercetin-bound protein were 16.76 Å and 16.31 Å, where cyrtominetin exhibited steadier trajectory, indicating significant stability and compactness within the protein active pocket. Similarly, syringetin, genistein, ombuin, and kaempferol bound to the target protein, the average Rg values were found to be 16.56, 16.57, 16.54, and 16.33 Å, respectively. In the whole simulation process, all systems of ligand-bound proteins became more compact than RANKL apo state, which indicated that the RANKL-flavonoids complexes are well converged.

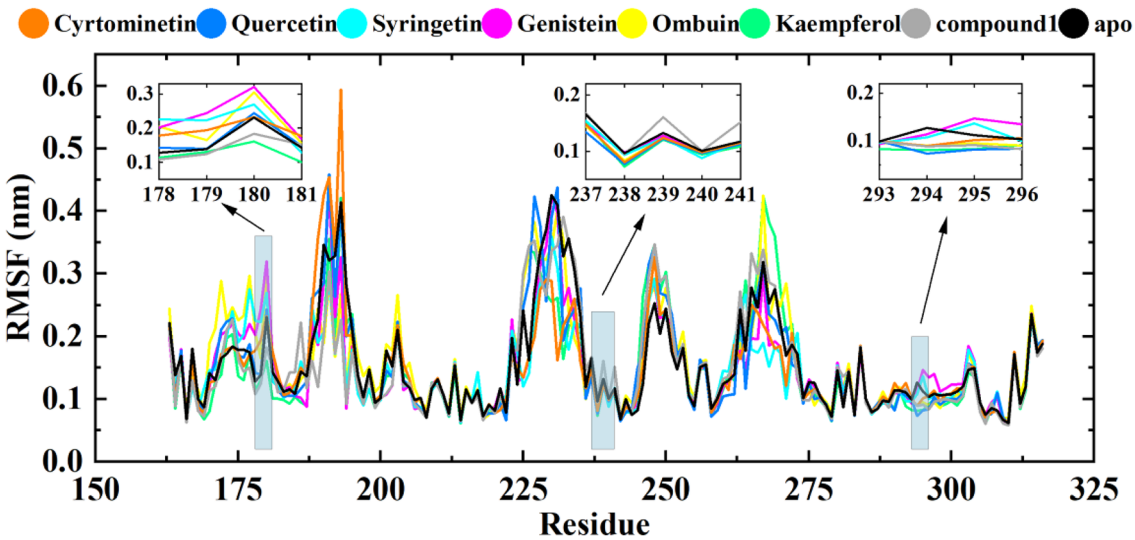

Fig. 5. Analysis of RMSF trajectories versus residue number of the RANKL-flavonoids complexes over 100 ns all-atom MD simulation.

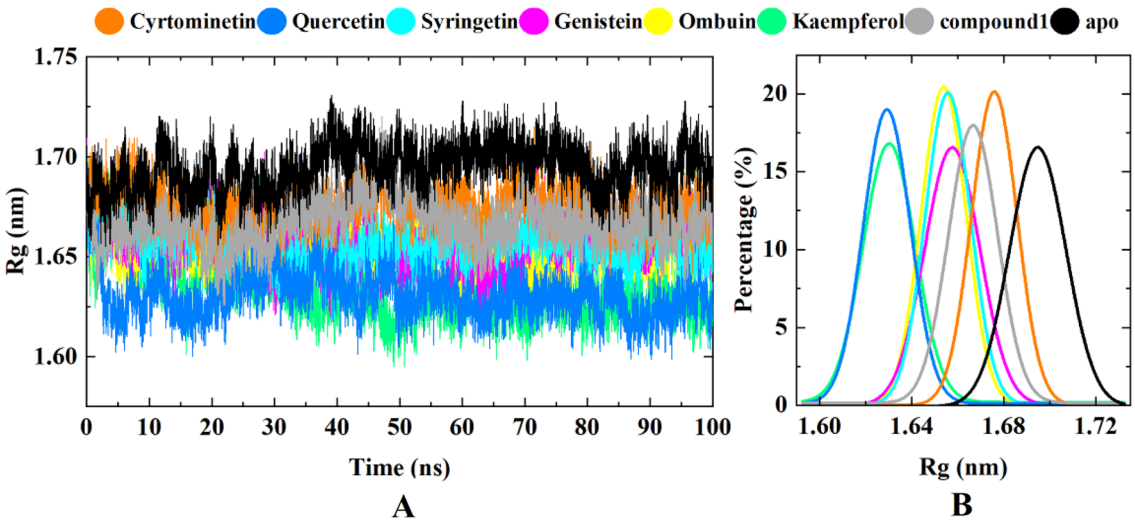

Fig. 6. Time evolution Rg trajectories of the RANKL-flavonoids complexes over 100 ns all-atom MD simulation. (**A**) The Rg of the RANKL-flavonoids complexes. (**B**) The relative frequency distribution of Rg.

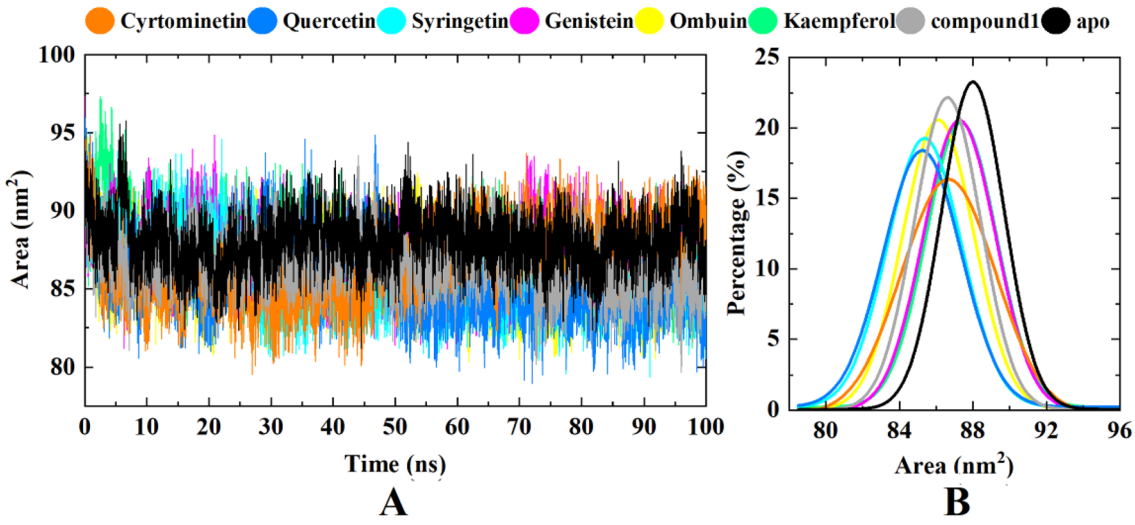

Fig. 7. Time evolution SASA trajectories of the RANKL-flavonoids complexes over 100 ns all-atom MD simulation. (**A**) The SASA of the RANKL-flavonoids complexes. (**B**) The relative frequency distribution of SASA.

Solvent-accessible surface area

Moreover, another important quantity that we measure and analyze to probe the conformational stability of the protein–ligand complex is SASA. The SASA values were analyzed to assess the complexes volume change through GROMACS "gmx sasa" script. Generally, SASA correlates for the molecular surface area being assessable to solvent molecules providing a quantitative measurement about the extent of protein/solvent interaction[38]. The decrease in SASA values indicates that the structures conformations of the complexes become more compact under the influence of solvent-induced surface charges, resulting in increased stability.

As predicted, the SASA values of all RANKL-flavonoids complexes were comparable, and all values were concentrated between 85 to 90 nm^2 (Fig. 7). Among them, cyrtominetin-bound protein had a higher SASA trajectory in the initial phase. After this stage, the SASA value gradually decreased to reach min SASA value which was followed by a subsequent increase until reaching the end of the MD simulation run (average 86.68 nm^2). The elevated SASA trajectories might confer the migration of cyrtominetin towards the solvent side within the simulation time frames of 60 to 100 ns where the protein pocket became highly solvated and minimally compacted. The quercetin-bound protein showed lower SASA trajectory (average 85.56 nm^2), particularly within the last 50 ns. Such dynamic behavior suggested preferential confinement of quercetin within the protein pocket. The syringetin-bound protein and ombuin-bound protein had higher SASA trajectories in the initial phase, followed by a lower value, and then maintained a stable SASA until the end of the simulation. The SASA

trajectories of genistein-bound protein and kaempferol-bound protein were similar, with less fluctuation during the simulation, indicating that the stability of these two complexes was less affected by the solvent. On the other hand, the RANKL apo state showed stable SASA trajectorie (average 88.05 nm^2) until reaching 100 ns of the simulation run. In the whole simulation process, all systems of ligand-bound proteins became more compact than RANKL apo state. In the presented study, findings from the SASA analysis appeared to ensure the well stability of the RANKL-flavonoids complexes previously presented by the Rg trajectory analysis.

Effects of flavonoids on the intra-chain interactions

To further explore the roles of flavonoids on the intra-chain interactions, the sidechain-sidechain contact diagrams of the RANKL monomer were calculated by using the GROMACS"gmx mdmat"program. As shown in Fig. 8, the contact distance between sidechains of residues in the RANKL monomer was represented by distinct colors. Blue and red expressed the distance between sidechains was 0.0 nm and 1.5 nm, respectively. When the color was closer to blue, the distance between the related sidechains was closer. On the contrary, when the color was closer to red, the related sidechains were farther from each other. In all simulation systems, the changes in contact distances were primarily localized in the active pocket. In the absence of flavonoids molecules, it was found that there was some repulsion between the sidechains of residues in the active pocket. In the presence of flavonoids molecules, it was observed that the number of blocks close to red was reduced, demonstrating that the contacts between sidechains were strengthened by flavonoids. To be more specific, the sidechain-sidechain contact distance between residues Ser294-Gln237, Ser294-Met239, Ser294-Tyr241, Asn295-Gln237, Asn295-Met239, Asn295-Tyr241, Gly178-Gln237, Gly178-Met239, Gly178-Tyr241, Ser179-Gln237, Ser179-Met239, and Ser179-Tyr241 was decreased by the presence of flavonoids. In addition, the sidechain-sidechain contact distance between most residues was still kept almost the same as the RANKL monomer without flavonoids molecules. The results of sidechain-sidechain contact maps indicated that flavonoids molecules promoted the sidechain-sidechain contacts in the active pocket, and then led to the formation of more compact conformation in the RANKL monomer, which were in good agreement with the results of Rg and SASA.

Hydrogen bonds analysis

Hydrogen bond interaction is one of the main parameters to reflect the stability of the ligand at the active pocket in the protein. It provides the basis for molecular recognition and selectivity by imparting directionality and explicitness to molecular interactions[39]. Thus, we performed H-bonds analysis using the GROMACS"gmx hbond"script to calculate the time evolution of hydrogen bonds during the entire MD simulation process (Fig. 9).

In complexes with cyrtominetin and quercetin, the most conformations formed 3 to 4 hydrogen bonds during the simulation. A very few conformations showed less than 2 and greater than 5 hydrogen bonds. In the complexes with syringetin and genistein, the conformational changes showed the same trend. However, in complexes with ombuin and kaempferol, the average number of hydrogen bonds formed was 1 to 3. These results provided a good verification for molecular docking. In comparison, compound 1 formed an average number of 2 to 3 hydrogen bonds in the first 50 ns, and few conformations showed up to 5 hydrogen bonds. In the last 50 ns, the number of hydrogen bonds decreased until reaching the end of the MD simulation run. Most flavonoids formed a higher number of hydrogen bonds inside the binding pocket throughout the simulation than control group. These results showed that the flavonoids were able to maintain strong interaction with the binding pocket of RANKL during the simulation.

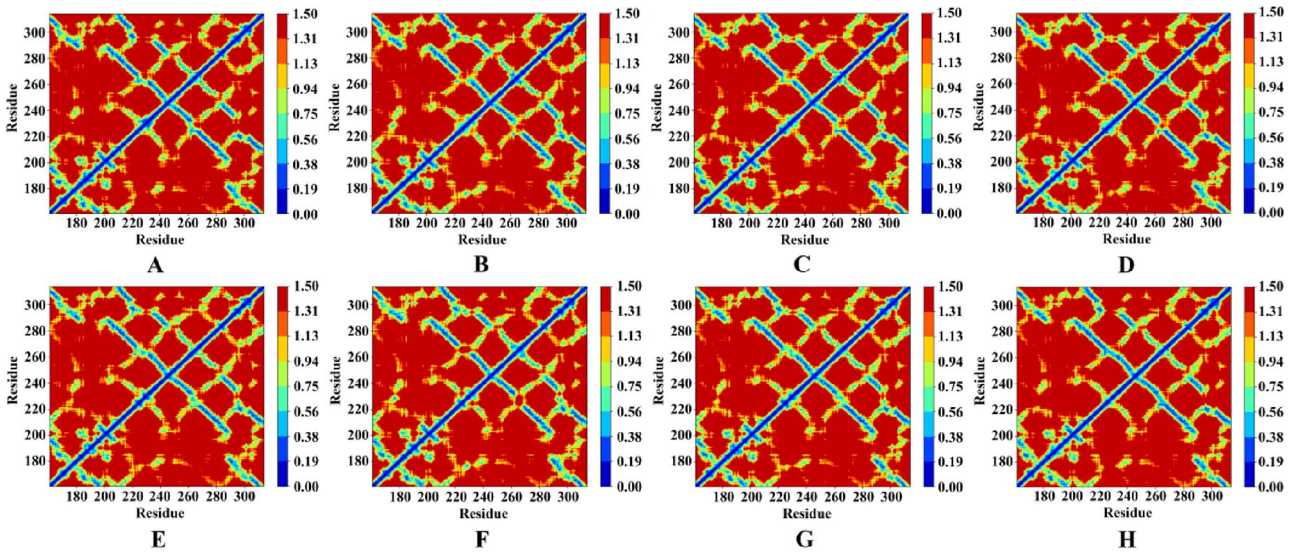

Fig. 8. The sidechain-sidechain contact maps for RANKL monomer of all flavonoids simulation systems. (**A**) Cyrtominetin, (**B**) Quercetin, (**C**) Syringetin, (**D**) Genistein (**E**) Ombuin (**F**) Kaempferol (**G**) control group and (**H**) apo. The distance is given in nm and indicated by the color code.

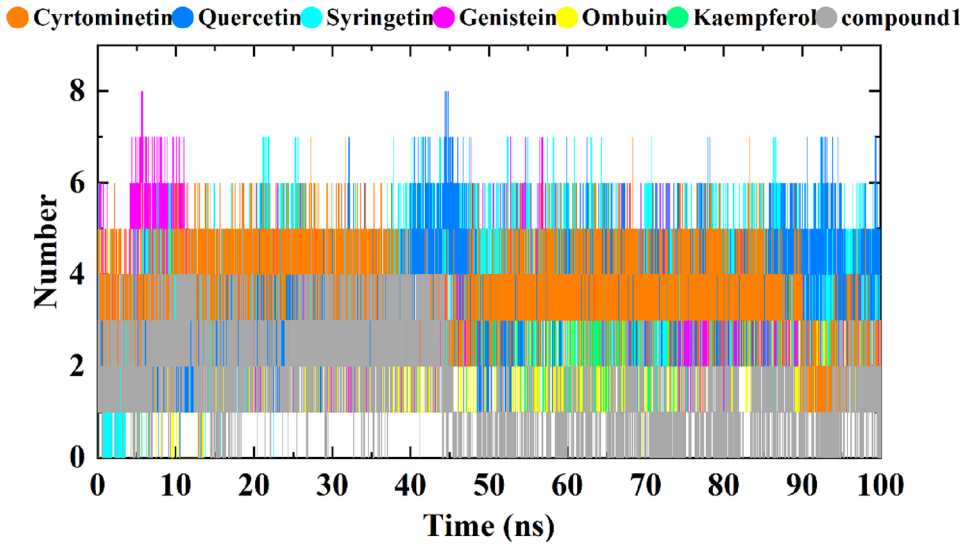

Fig. 9. Time evolution plot of hydrogen bond interaction between the RANKL and flavonoids over 100 ns all-atom MD simulation.

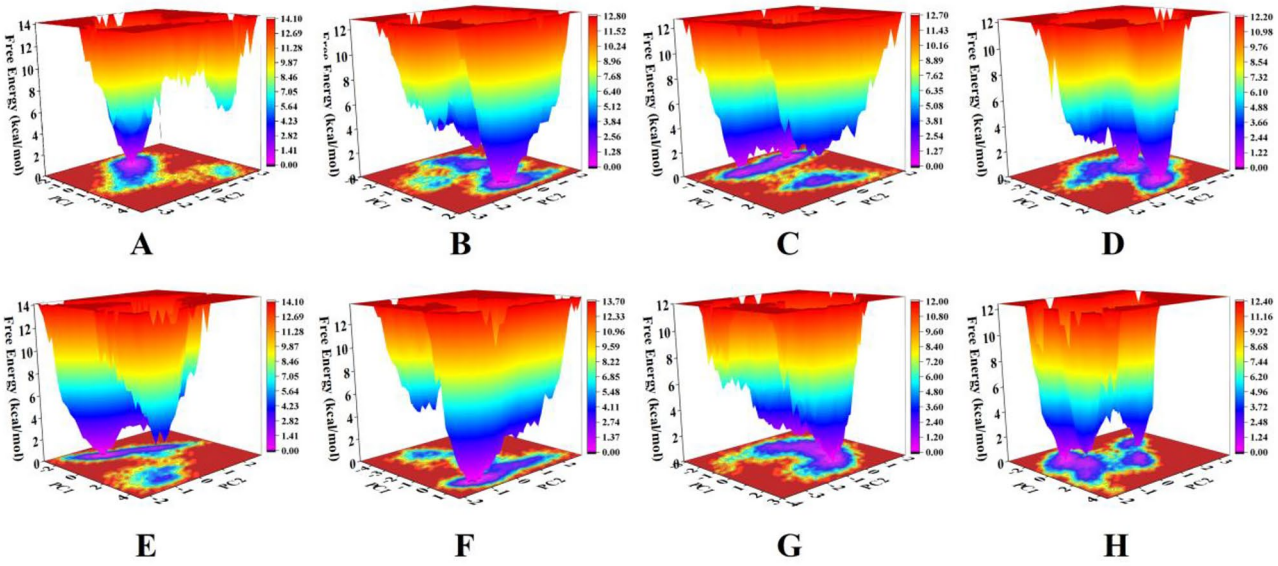

Fig. 10. FEL of RANKL-flavonoids complexes. (**A**) Cyrtominetin, (**B**) Quercetin, (**C**) Syringetin, (**D**) Genistein, (**E**) Ombuin, (**F**) Kaempferol, (**G**) control group, and (**H**) apo. The free energy is given in kcal/mol and indicated by the color code, from lower to higher energy in the right panel.

Free energy analyses

Principal component analyses (PCA) of MD simulations is a technique used to reveal various conformations of protein molecules. Protein function is regulated by the transformation between various conformations. To make proteins functional, reasonable flexibility and rigidity are required, especially for the residues in the binding site. Typically, tighter interactions would limit the movement of the protein, so it is not allowed to switch some conformations required for its activity[40].

In order to understand the transformation of protein occupied in the conformational space, we applied PCA to analyze the combined fluctuations in the most unstable regions of the protein molecule into two variables, principal component 1 (PC1) and principal component 2 (PC2), which represent most of the fluctuations observed during MD simulation. Next, FEL plots were generated from the principal PC1 and principal PC2 coordinates. The FEL accurately described the minimum energy conformation ensembles of proteins, which is crucial for understanding the conformational transition underlying protein–ligand interactions. Figure 10 showed that the binding of flavonoids with RANKL occurs through the minimum free energy pathway. The FEL of RANKL-cyrtominetin complex showed that the stably bound conformation was widely filled to a

single consolidated energy minimum, which provided favorable evidence for interaction inducing the stable conformational transition of the complex. The FEL of RANKL-quercetin complex showed the appearance of two distinct populations confined to two different energy basins, separated with high transition barrier >4.8 kcal/mol, which signified the population of loosely and tightly ligand-bound conformations of the protein. The conformational ensemble derived from FEL showed that the complexes of RANKL-syringetin and RANKL-genistein clustered in the different energy basins. However, these energy minima separated through a low transition barrier <3.0 kcal/mol indicated that the ensemble states of complexes readily transferred from one energy basin to another with a small deviation. The FEL with segmented small energy of complexes with ombuin and kaempferol indicated the presence of loosely bound complexes. The low transition barriers between small energy basins suggested a longer equilibration phase of the complex structure. Contrary to this, RANKL apo state experienced a wide region of phase space. In fact, it explored a large conformational space in comparison to the other RANKL-flavonoids complexes, which represent the overall higher flexibility of the protein. The conformational ensemble occupying the small energy basin represented the population of the equilibration phase, which readily achieved a stable equilibrium. It is apparent from these plots that RANKL-flavonoids complexes are localized in a small conformational space, which may facilitate the vital interactions with flavonoids.

Secondary structural characterization

Although the above results indicated that the conformation of RANKL monomer was stabilized by the presence of flavonoids, the detailed mechanisms of the interactions between RANKL monomer and flavonoids were still unclear. Therefore, to further explore the effects of flavonoids on the secondary structure of the RANKL monomer, we conducted structural analysis using DSSP algorithm.

The secondary structure information for each residue (residues 162–317) during the simulations was given in Fig. 11. For the RANKL monomer without flavonoids molecules, most of the residues mainly kept the β-sheet structure throughout the whole simulation. Among them, the residues Gly178-Lys181 in the N-terminal of RANKL monomer were converted into short β-sheet structure connected with bend structure. The residues Gln237-Tyr241 always kept the β-sheet structure throughout the whole 100 ns simulation. In the C-terminal of RANKL monomer, the residues Val293-Pro296 kept the 3-helix structure, with occasional local deviations that converted the 3-helix to turn structure. By comparison, the time evolution of the secondary structures of RANKL monomer in the presence of flavonoids molecules is not significantly different from that of RANKL monomer alone, indicating that the RANKL-flavonoids complexes are rather stable, which is well consistent with the previous analysis.

Effects of flavonoids on the binding free energy of RANKL monomer

The binding free energy provides a relatively comprehensive assessment of the binding affinity between receptors and ligands, which takes various interaction forces into account[41]. Previous study indicated that a negative binding free energy value represents favorable ligand-receptor binding[42]. To obtain quantitative insights into the interactions between RANKL monomer and flavonoid molecules, we calculated the binding free energy of RANKL-flavonoids complexes using MM-PBSA method. The binding free energy and various contribution terms for RANKL-flavonoids complexes were summarized in Table 2. It was clearly observed that both non-bonded electrostatics interactions (ΔE_{elec}) and non-bonded vdW interactions (ΔE_{vdW}) favored the interactions between RANKL monomer and flavonoids molecules. And the nonpolar solvation free energy ($\Delta G_{nonpolar\text{-}sol}$) was also favorable for the formation of RANKL-flavonoids complexes. However, the polar solvation free energy ($\Delta G_{polar\text{-}sol}$) was unfavorable. The polar binding free energy ΔG_{polar} was the sum of $\Delta G_{polar\text{-}sol}$ and ΔE_{elec}, and

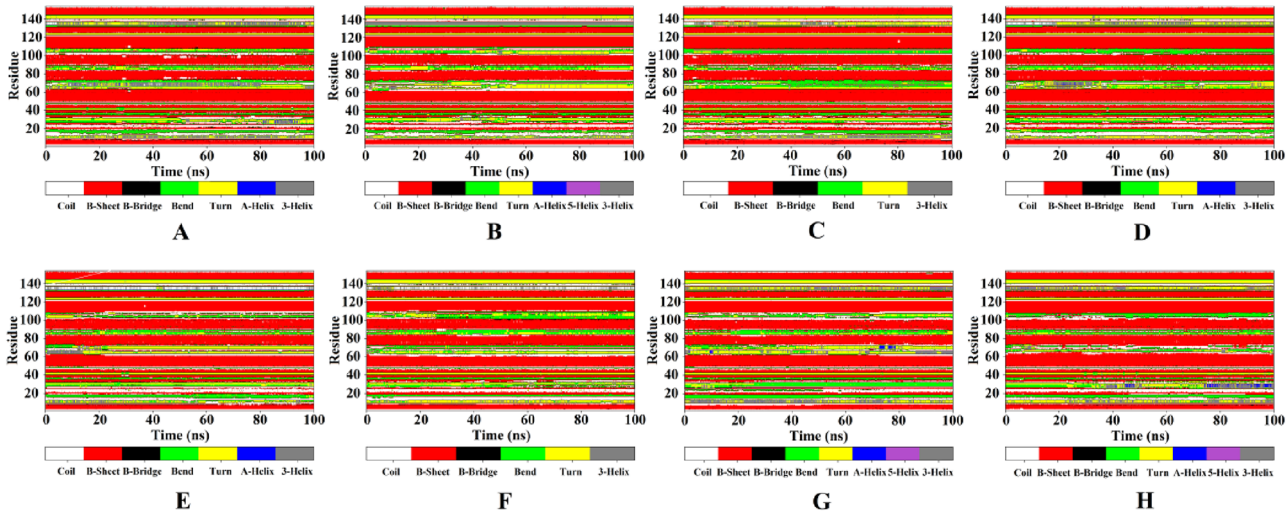

Fig. 11. Time evolution secondary structures of the RANKL-flavonoids complexes over 100 ns all-atom MD simulation. (**A**) Cyrtominetin, (**B**) Quercetin, (**C**) Syringetin, (**D**) Genistein, (**E**) Ombuin, (**F**) Kaempferol, (**G**) control group, and (**H**) apo.

Energy terms	Control group	Cyrtominetin	Quercetin	Syringetin	Genistein	Ombuin	Kaempferol
$\triangle E_{elec}$(kJ/mol)	−31.173±15.451	−122.668±14.010	−104.110±20.859	−137.866±20.612	−136.358±22.337	−51.541±11.696	−80.534±11.510
$\triangle E_{vdW}$(kJ/mol)	−102.152±16.511	−85.806±19.310	−64.291±16.876	−87.556±14.752	−72.592±14.764	−52.015±14.495	−78.970±13.591
$\triangle E_{MM}$(kJ/mol)	−133.325	−208.474	−168.401	−225.423	−208.950	−118.556	−159.504
$\triangle G_{polar\text{-}sol}$(kJ/mol)	101.112±24.155	171.266±19.677	135.083±18.764	209.349±21.194	180.071±20.034	66.493±14.658	125.323±11.237
$\triangle G_{nonpolar\text{-}sol}$(kJ/mol)	−13.262±2.024	−12.997±0.853	−11.020±2.102	−13.656±0.930	−13.219±0.879	−8.374±2.694	−12.320±0.655
$\triangle G_{polar}$(kJ/mol)	69.939	48.599	30.974	71.482	43.713	14.592	44.789
$\triangle G_{nonpolar}$(kJ/mol)	−115.414	−98.803	−75.311	−101.212	−85.811	−60.388	−91.290
$\triangle G_{binding}$(kJ/mol)	−45.475±19.837	−50.205±15.845	−44.338±18.939	−29.730±10.821	−42.098±16.920	−45.796±13.605	−46.502±11.988

Table 2. Binding free energy between RANKL monomer and flavonoids.

the nonpolar binding free energy $\Delta G_{nonpolar}$ was the sum of $\Delta G_{nonpolar\text{-}sol}$ and ΔE_{vdW}. The ΔG_{polar} and $\Delta G_{nonpolar}$ represented the net results of polar interactions and nonpolar interactions, respectively. Hence, the results indicated that the nonpolar interactions were involved in the stabilization of RANKL-flavonoids complexes. Although, ΔG_{polar} impaired the binding, the unfavorable change in the polar binding free energy was completely compensated by $\Delta G_{nonpolar}$.

To further quantify the energetic contributions of binding pocket residues to the interactions between flavonoids and RANKL monomer, we performed per-residue free energy decomposition (Fig. 12). The binding interaction with cyrtominetin showed that the amino acid residues, Gly178, Ser179, His180, Met239, Tyr241, Ser294, and Pro296, contributed the most to the total ΔGbinding. Although the vdW interaction primarily stabilized the cyrtominetin at the binding pocket, the electrostatic interaction also contributed to the observed stability by His180 (− 3.21 kcal/mol), Lys181 (−3.89 kcal/mol), and Ser294 (− 8.63 kcal/mol), respectively. Quercetin was predominantly stabilized in the binding pocket through the electrostatic interaction, which was mostly contributed by the residues Ser179 (− 2.21 kcal/mol), Gln237 (− 2.85 kcal/mol), Ser294 (− 6.72 kcal/mol), and Asn295 (− 9.48 kcal/mol), respectively. The free energy decomposition plot of syringetin indicated that amino acids Gly178, His180, Met239, and Tyr241 were important for the binding of syringetin at the binding pocket. Surprisingly, it is noted that Lys181 contributed to both electrostatic energy (− 13.24 kcal/mol) and vdW energy (− 7.40 kcal/mol). The favorable binding of genistein showed the significant contribution of residues, Gly178, Lys181, Ser294, and Pro296. It is noted that Gln237 and Asn295 contributed higher electrostatic energy (− 5.83 and −5.67 kcal/mol, respectively). The plot of free energy decomposition analysis showed that the active site residues, Gly178, Ser179, His180, Lys181, Met239, Tyr241, and Asn295 favored the binding stability of ombuin. The binding interaction with kaempferol showed that the amino acid residues, Gly178, Ser179, His180, Met239, Tyr241, and Asn295, were important for the interaction in the binding pocket. Interestingly, it is noted that Tyr241 contributed higher electrostatic energy (− 5.67 kcal/mol), whereas the maximum vdW energy (− 7.97 kcal/mol) was contributed by His180. control group was predominantly stabilized in the binding pocket through the vdW interaction, which was mostly contributed by the residues Ser179 (− 5.36 kcal/mol), His180 (− 4.68 kcal/mol), Lys181 (− 4.66 kcal/mol) Gln237 (− 10.88 kcal/mol) and Asn295 (− 4.07 kcal/mol), respectively. However, the binding pocket of RANKL consisted of hydrophilic and hydrophobic residues. Thus, we observed that both electrostatic energy and vdW energy were major contributions to stabilizing the ligand interaction.

Discussion

Osteoporosis, recognized as the most prevalent metabolic bone disorder, is closely associated with the abnormal activation of RANKL/RANK/OPG signaling pathway[43],[44]. Contemporary research has demonstrated that flavonoid compounds exhibit significant inhibitory effects on RANKL-mediated osteoclastogenesis, although their precise molecular mechanisms remain to be fully characterized[22–24]. EU, a traditional medicinal plant extensively employed in the management of bone-related pathologies, contains bioactive flavonoids that are postulated to constitute the principal pharmacologically active constituents[30]. Based on these considerations, the present investigation employed molecular simulation approaches to comprehensively elucidate the structural basis of molecular recognition between bioactive flavonoids derived from EU and RANKL protein.

The molecular docking results demonstrated that all six tested flavonoids exhibit strong binding affinities to RANKL, with cyrtominetin showing particularly remarkable binding energy (−50.205 kJ/mol). Detailed analysis revealed that these compounds share a common binding mode, primarily interacting with the loops AA' region of RANKL (residues 179–181). This region has been previously identified as critical for RANKL-RANK interaction, suggesting that flavonoid binding may competitively inhibit this key signaling pathway[32]. The conserved hydrogen bonding interactions with Gly178 and Asn295 are particularly noteworthy, as these residues form part of the structural core that maintains RANKL's functional conformation. Furthermore, the π-π stacking interactions observed with His180 and Tyr241 contribute additional stabilization energy, consistent with the known importance of aromatic interactions in protein–ligand binding[45].

The molecular dynamics simulations provided critical insights into the dynamic behavior and structural stability of flavonoid-RANKL complexes. Our 100-ns all-atom simulations demonstrated that all systems achieved thermodynamic equilibrium within 15–30 ns, with the cyrtominetin-RANKL complex showing exceptional stability (average Cα-RMSD of 2.86 Å). RMSF analysis showed binding site residues (178–181, 237–241, 293–296) exhibited reduced flexibility (ΔRMSF = −0.5 to −1.2 Å), while distal loops displayed increased mobility, a pattern characteristic of functional protein–ligand complexes[46]. Principal component

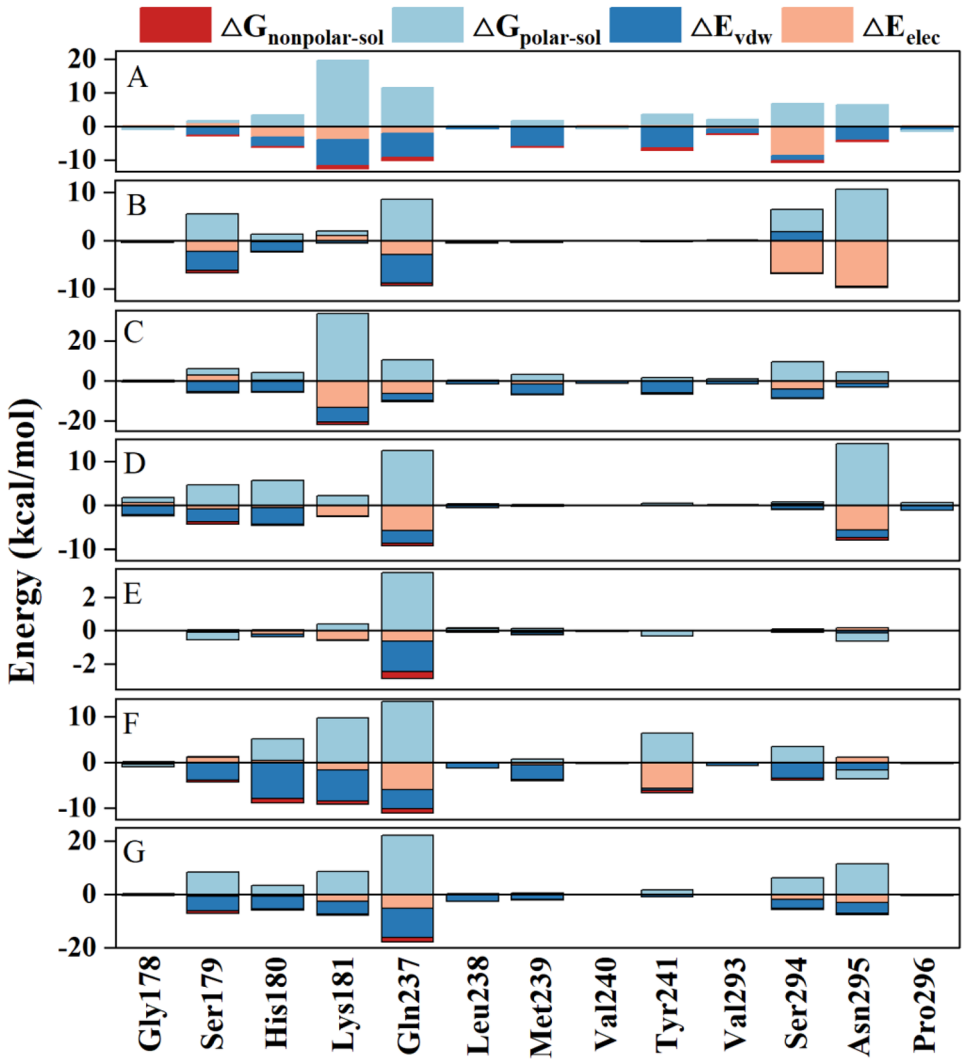

Fig. 12. The residue decomposition plot (MM-PBSA) representing the binding energy contribution of the residues energetically stabilizing the flavonoids at binding pocket. (**A**) Cyrtominetin, (**B**) Quercetin, (**C**) Syringetin, (**D**) Genistein, (**E**) Ombuin, (**F**) Kaempferol and (**G**) control group.

analysis revealed that flavonoid binding reduced RANKL's conformational space while specifically stabilizing the functionally important loop region. Secondary structure analysis confirmed maintenance of RANKL's structural integrity, with the central β-sheet core remaining intact and the Gly178-Lys181 β-sheet showing enhanced stability (98% occupancy in cyrtominetin complex). This finding aligns with recent work on small molecule inhibitors of RANKL-RANK interaction[47]. Solvent accessibility decreased in all complexes (ΔSASA = −2 to −4 nm^2), with cyrtominetin inducing the most consistent desolvation. Hydrogen bond analysis revealed cyrtominetin maintained 3–4 stable hydrogen bonds, with key interactions to Gly178 and Asn295 persisting for > 85% of the simulation. These dynamic observations collectively suggest that flavonoid binding, particularly by cyrtominetin, stabilizes RANKL's binding interface while preserving global structure, providing a molecular basis for competitive inhibition of RANKL. The robust stability and balanced interaction profile of cyrtominetin-RANKL complex highlights its potential as a lead compound for further development.

The MM-PBSA calculations provided crucial thermodynamic insights into flavonoid-RANKL binding interactions, revealing that nonpolar interactions (vdW and hydrophobic effects) accounted for approximately 70% of the total binding energy, consistent with the predominantly hydrophobic nature of the binding pocket, while electrostatic interactions—particularly those involving key residues Lys181 and Asn295—contributed the remaining 30% of binding energy. Per-residue energy decomposition analysis identified Gly178, Ser179 and His180 as major energetic contributors, with His180 demonstrating particularly strong electrostatic stabilization (−3.21 kcal/mol in the cyrtominetin complex). These computational findings not only corroborate previous experimental studies on flavonoid-mediated inhibition of osteoclastogenesis, but more importantly establish a comprehensive thermodynamic framework for understanding the atomic-level mechanisms underlying their biological activity[48–50].

Compared to existing therapies like denosumab, the identified flavonoid scaffolds offer potential advantages including smaller molecular size for improved bioavailability, precise targeting of functional residues, and multi-target potential through modulation of NF-κB, MAPK, and AKT pathways[30]. The study validates traditional medicinal use of EU while providing a detailed interaction map for structure-based drug design. Future work should focus on structural studies of complexes, and medicinal chemistry optimization to enhance therapeutic potential. These findings significantly advance our understanding of flavonoid-RANKL interactions and establish cyrtominetin as a promising lead compound for developing novel anti-osteoporotic agents.

Conclusion

In summary, using molecular docking and classical MD simulation, we investigated the potential of 6 flavonoids to bind in the active site of the RANKL protein. The selected molecules exhibited variable degrees of binding affinities toward the RANKL monomer in molecular docking simulation. We found that most flavonoids formed strong hydrogen bonds with Gly178 and Asn195 in RANKL monomer, resulting in higher binding affinity. These interactions were assumed to be essential for the activity, along with significant extra interactions with other binding residues. The identification of key RANKL residues suggested that designing small molecules targeting these residues could be a promising strategy for modulating RANKL activity. Furthermore, cyrtominetin may serve as a promising lead compound for developing potent RANKL inhibitors. These findings could facilitate the development of novel therapeutic agents targeting RANKL for treating bone-related diseases. Furthermore, the MD simulation showed favorable interactions between the selected molecules and the active site of RANKL monomer. Throughout the 100 ns all-atom MD simulation, flavonoids exhibited superior stability at the RANKL binding site for over 70 ns, during which the solvation energy was largely compensated by electrostatic and vdW binding energies.

Materials and methods

Ligand preparation

The ADMET properties of all flavonoids were determined by the online in-silico prediction model ADMETlab 2.0 (https://admetmesh.scbdd.com/)[51], such as absorption, distribution, metabolism, excretion, toxicity and physicochemical properties. Additionally, drug similarity properties were evaluated using the Lipinski rule. Then, the 2D structures of compounds meeting the rules were retrieved from PubChem in SDF file format, while the 3D structures conversion and energy minimization were performed by applying standard geometric parameters of the molecular modeling software package Sybyl-X (version 2.1.1, Tripos Inc.). Tripos force field and Powell conjugate gradient algorithm were employed to minimize the energy of each compound using 0.05 kcal/mol Å and Gasteiger- Huckel charges as convergence criteria[52].

Protein preparation

This study employed the crystal structure of human RANKL/OPG-CRD complex (PDB: 3URF) as the docking template, selected for its high resolution (2.7 Å), complete binding interface information (99.9% structural completeness), and experimentally validated key interaction residues. The critical role of these residues was confirmed by SPR assays (KD = 0.65 nM) and mutagenesis studies (Glu95 Ala mutation significantly reduced binding affinity), thereby establishing this structure as a reliable model for studying competitive inhibition mechanisms. Next, the crystal structure of 3URF was extracted from Protein Data Bank (PDB https://www.rcsb.org) in PDB file format[32]. In the process of protein preparation, water molecules were removed from the structure, H atoms were added, and side chains were fixed. Protein structure minimization was performed using Tripos force field and partial atomic charges were calculated the Gasteiger- Huckel method. Finally, the optimal protein structure was verified by PROCHECK tool (https://saves.mbi.ucla.edu/) to determine the allowable regions for torsion angles ψ against φ of amino acid residues[53].

Binding site prediction

Based on the analysis of the interaction surface, the most suitable concave pocket for molecular docking was chosen as the binding site[32,33]. Sybyl-X was used to generate the binding site of the protein, which provides a pocket for binding the ligand molecule and offers the expected active region.

Molecular docking

The Surflex-Dock module in Sybyl-X was used to evaluate the interactions of the flavonoids against RANKL, where 20 possible conformations for each docked ligand were produced. The docked conformations were evaluated and ranked using the Total_Score function, which was expressed in -log10(Kd) units to represent binding affinities. Binding site conformations were selected based on Total_Score values, with the highest-scoring conformation identified as the optimal structure for docking mode analysis. In general, Total_Score > 4.0 indicates certain binding activity, Total_Score > 5.0 indicates good binding activity, while Total_Score > 7.0 indicates strong binding activity[54]. Additionally, previous studies identified a lead compound, which can directly bind to RANKL and has the property of inhibiting RANKL/RANK protein interaction[33]. Therefore, it was used as a control group for comparison with flavonoids. Subsequently, PyMOL 2.4 program[55] and Discovery Studio Visualizer 2021[56] were employed to visualize the binding mode between the protein and ligand.

Molecular dynamics simulations

Molecular docking provides static position of the most favorable conformations of molecules in the protein binding pocket to present a stable complex. However, static images are not able to present other crucial features involved in protein stability, including the flexibility of residues and secondary structural elements[57]. Likewise,

the conformational changes caused by the dynamic behavior of proteins may affect their actual biological functions[58]. To investigate dynamic behavior of flavonoids at the binding pocket of RANKL, the molecular dynamic (MD) simulation was executed. Before MD simulation, the selected compounds were prepared using ATB online server (https://atb.uq.edu.au/) to generate the initial topology[59]. The simulation was performed using the GROMACS 2019.6[60]. GROMOS96 54a7 force field was applied to the system, and a dodecahedron water box composed of TIP3P water model was used to solvate the system[61]. Na^+ and Cl^- ions were added to the box to neutralize the overall system. Next, the steepest descent minimization algorithm was used to carry out energy minimization at 50,000 steps. The process of energy minimization was to eliminate the negative interaction in the system. Then, the system was heated gradually at 300 K using 100 ps in the NVT canonical ensemble with 2 fs time step. For the NPT isothermal–isobaric ensemble, the atoms were relaxed at 300 K and 1 bar using 100 ps with 2 fs time step. To treat long-range electrostatic interactions, the Particle Mesh Ewald (PME) method was used[62]. After equilibrating the system at 300 K temperature and 1 bar pressure, the MD run for the system was carried out at 100 ns with 2 fs time step at 50,000,000 steps. Various structural parameters were calculated using GROMACS tools to characterize protein–ligand complex dynamics, including root mean square deviation (RMSD), root mean square fluctuation (RMSF), radius of gyration (Rg), solvent accessible surface area (SASA), intermolecular hydrogen bonds (H-bonds), intra-chain interactions, secondary structural characterization, and free energy landscape (FEL).

Binding free energy estimation

Free energy calculation analysis is a useful method to quantitatively estimate the binding affinity between biomacromolecules and ligands[63]. In the present study, the binding free energy of protein–ligand complex was evaluated using molecular mechanics Poisson Boltzmann surface area (MM-PBSA), which described the structural and molecular stability of the ligand in the active site[64]. According to the MM-PBSA method, the calculation principle of the binding free energy of protein–ligand complex was summarized as following:

$$\Delta G_{\mathrm{binding}} = \Delta G_{\mathrm{complex}} - (\Delta G_{\mathrm{receptor}} + \Delta G_{\mathrm{ligand}})$$

where $\Delta G_{complex}$, $\Delta G_{receptor}$ and ΔG_{ligand} were the binding free energy for RANKL-flavonoids complexes, RANKL monomer, and flavonoids molecules, respectively. Excluding the entropy term (TΔS), the above equation for the binding free energy could be approximately written as,

$$\Delta G_{\mathrm{binding}} = \Delta E_{\mathrm{MM}} + \Delta G_{\mathrm{solvation}}$$

where ΔE_{MM} was the change in the average molecular mechanics interaction energy upon ligand binding and $\Delta G_{solvation}$ was the change in solvation free energy upon ligand binding. The change of average molecular mechanics potential energy (ΔE_{MM}) in vacuum was estimated by:

$$\Delta E_{\mathrm{MM}} = \Delta E_{\mathrm{intern}} + \Delta E_{\mathrm{elec}} + \Delta E_{\mathrm{vdw}}$$

where ΔE_{intern} was the change of molecular internal energy, including the energy of bond, angle, dihedral, and improper interactions. Generally, ΔE_{intern} was assumed to be zero. The ΔE_{elec} and ΔE_{vdw} were electrostatic interaction energy and vdW interaction energy, respectively. Further, $\Delta G_{solvation}$ could be written as,

$$\Delta G_{\mathrm{solvation}} = \Delta G_{\mathrm{polar-sol}} + \Delta G_{\mathrm{nonpolar-sol}}$$

where $\Delta G_{polar\text{-}sol}$ was the change in the polar part of the solvation free energy, and $\Delta G_{nonpolar\text{-}sal}$ was the change in the non-polar part of the solvation free energy upon ligand binding to the proteins. $\Delta G_{polar\text{-}sol}$ was calculated by using the PB equation and $\Delta G_{nonpolar\text{-}sol}$ was estimated as a function of the SASA as the equation following:

$$\Delta G_{\mathrm{nonpolar-sol}} = \gamma \mathrm{SASA} + \beta$$

where γ was the coefficient related to the surface tension of the solvent and β was the fitting parameter.

The binding free energy was calculated by the g_mmpbsa tool of GROMACS. The default parameters for γ and β were used in the g_mmpbsa tool. In the equilibrium phase of molecular dynamics simulation, the binding free energy was calculated by extracting 20 snapshots from 60 to 80 ns in a time interval of 1 ns.

Data availability

The datasets used and/or analyzed during the current study available from the corresponding author on reasonable request.

Received: 27 January 2025; Accepted: 9 May 2025
Published online: 17 May 2025

References

1. Gullberg, B., Johnell, O. & Kanis, J. A. World-Wide projections for hip fracture. *Osteoporos. Int.* **7**, 407–413 (1997).
2. Kanis, J. A. Assessment of fracture risk and its application to screening for postmenopausal osteoporosis: Synopsis of a WHO report. *WHO Study Group. Osteoporos. Int.* **4**, 368–381 (1994).
3. Florencio-Silva, R., Sasso, G. R., Sasso-Cerri, E., Simoes, M. J. & Cerri, P. S. Biology of bone tissue: Structure, function, and factors that influence bone cells. *Biomed Res. Int.* **2015**, 421746 (2015).

4. Kim, B., Lee, K. Y. & Park, B. Icariin Abrogates osteoclast formation through the regulation of the RANKL-Mediated TRAF6/NF-Kappab/ERK Signaling Pathway in Raw264.7 Cells. *Phytomedicine* **51**, 181–190 (2018).
5. Kawatani, M. et al. The identification of an osteoclastogenesis inhibitor through the inhibition of glyoxalase I. *Proc. Natl. Acad. Sci. U. S. A.* **105**, 11691–11696 (2008).
6. Wittrant, Y. et al. Regulation of Osteoclast Protease Expression by RANKL. *Biochem. Biophys. Res. Commun.* **310**, 774–778 (2003).
7. Zou, B. et al. Kirenol Inhibits RANKL-Induced osteoclastogenesis and prevents ovariectomized-Induced osteoporosis Via suppressing the Ca2+-NFATc1 and Cav-1 signaling pathways. *Phytomedicine* **80**, 153377 (2021).
8. Cho, E. et al. PMSA prevents osteoclastogenesis and Estrogen-dependent bone loss in mice. *Bone* **142**, 115707 (2021).
9. Chen, H. et al. Neobavaisoflavone inhibits osteoclastogenesis through blocking RANKL signalling-mediated TRAF6 and C-Src recruitment and NF-Kappab, MAPK and Akt pathways. *J. Cell. Mol. Med.* **24**, 9067–9084 (2020).
10. Lee, J. et al. Lumican Inhibits Osteoclastogenesis and Bone Resorption by Suppressing Akt Activity. *Int. J. Mol. Sci.* **22**, 4717 (2021).
11. Lee, J. et al. PDK2 Deficiency Prevents Ovariectomy-Induced Bone Loss in Mice by Regulating the RANKL-NFATc1 Pathway During Osteoclastogenesis. *J. Bone. Miner. Res.* **36**, 553–566 (2020).
12. Willard, D. et al. Expression, Purification, and Characterization of the Human Receptor Activator of NF-Kappab Ligand (RANKL) Extracellular Domain. *Protein. Expr. Purif.* **20**, 48–57 (2000).
13. Tanaka, S. Signaling Axis in Osteoclast Biology and Therapeutic Targeting in the RANKL/RANK/OPG System. *Am. J. Nephrol.* **27**, 466–478 (2007).
14. Ji, X., Chen, X. & Yu, X. MicroRNAs in Osteoclastogenesis and Function: Potential Therapeutic Targets for Osteoporosis. *Int. J. Mol. Sci.* **17**, 349 (2016).
15. Cummings, S. R. et al. Denosumab for prevention of fractures in postmenopausal women with osteoporosis. *N. Engl. J. Med.* **361**, 756–765 (2009).
16. Setsu, N. et al. Severe hypercalcemia following denosumab treatment in a juvenile patient. *J. Bone Miner. Metab.* **34**, 118–122 (2016).
17. Vanderkerken, K. et al. Recombinant osteoprotegerin decreases tumor burden and increases survival in a murine model of multiple myeloma. *Cancer Res.* **63**, 287–289 (2003).
18. Feeley, B. T. et al. Mixed metastatic Lung Cancer lesions in bone are inhibited by noggin overexpression and Rank: Fc Administration. *J. Bone. Miner. Res.* **21**, 1571–1580 (2006).
19. Ta, H. M. et al. Structure-Based development of a receptor activator of nuclear Factor-Kappab Ligand (RANKL) inhibitor peptide and molecular basis for Osteopetrosis. *Proc. Natl. Acad. Sci. U. S. A.* **107**, 20281–20286 (2010).
20. Xu, H. et al. Niloticin Inhibits Osteoclastogenesis by Blocking RANKL-RANK interaction and suppressing the AKT, MAPK, and NF-Kappab signaling pathways. *Biomed. Pharmacother.* **149**, 112902 (2022).
21. Xu, H. et al. Ellagic Acid Blocks RANKL-RANK interaction and suppresses RANKL-Induced Osteoclastogenesis by Inhibiting RANK Signaling Pathways. *Chem. Biol. Interact.* **331**, 109235 (2020).
22. Jia, L. et al. Total flavonoids from celery suppresses RANKL-Induced osteoclast differentiation and bone resorption function Via attenuating NF-Kb and P38 pathways in RAW2647 Cells. *J. Funct. Foods.* **69**, 103949 (2020).
23. Wattel, A. et al. Flavonoid quercetin decreases osteoclastic differentiation induced by RANKL Via a mechanism involving NF Kappa B and AP-1. *J. Cell. Biochem.* **92**, 285–295 (2004).
24. Sekaran, S., Roy, A. & Thangavelu, L. Re-appraising the role of flavonols, flavones and flavonones on osteoblasts and osteoclasts- A review on its molecular mode of action. *Chem. Biol. Interact.* **355**, 109831 (2022).
25. Masuhara, M. et al. A Relation between osteoclastogenesis inhibition and membrane-type estrogen receptor GPR30. *Biochem. Biophys. Rep.* **8**, 389–394 (2016).
26. Lee, W., Lee, E., Sung, M. & Yoo, W. Kaempferol inhibits IL-1Beta-Stimulated, RANKL-Mediated osteoclastogenesis Via downregulation of MAPKs, C-Fos, and NFATc1. *Inflammation* **37**, 1221–1230 (2014).
27. Pang, J. L. et al. Differential activity of kaempferol and quercetin in attenuating tumor necrosis factor receptor family signaling in bone cells. *Biochem. Pharmacol.* **71**, 818–826 (2006).
28. Karieb, S. & Fox, S. W. Phytoestrogens directly inhibit tnf-alpha-induced bone resorption in RAW264.7 cells by suppressing C-Fos-induced NFATc1 expression. *J. Cell. Biochem.* **112**, 476–487 (2011).
29. Tsai, Y. et al. Syringetin suppresses osteoclastogenesis mediated by osteoblasts in Human Lung adenocarcinoma. *Oncol. Rep.* **34**, 617–626 (2015).
30. Feng, S. et al. Exploring the potential therapeutic effect of eucommia ulmoides-dipsaci radix herbal pair on osteoporosis based on network pharmacology and molecular docking technology. *RSC Adv.* **12**, 2181–2195 (2022).
31. Zhu, W., Khalifa, I., Peng, J. & Li, C. Position and orientation of gallated proanthocyanidins in lipid bilayer membranes: influence of polymerization degree and linkage type. *J. Biomol. Struct. Dyn.* **36**, 2862–2875 (2018).
32. Luan, X. et al. Crystal structure of human rankl complexed with its decoy receptor osteoprotegerin. *J. Immunol.* **189**, 245–252 (2012).
33. Jiang, M. et al. Development of small-molecules targeting receptor activator of nuclear factor-kappab ligand (RANKL)-Receptor activator of nuclear factor-kappab (RANK) protein-protein interaction by structure-based virtual screening and hit optimization. *J. Med. Chem.* **62**, 5370–5381 (2019).
34. Karplus, M. & Petsko, G. A. Molecular Dynamics Simulations in Biology. *Nature* **347**, 631–639 (1990).
35. Schreiner, W., Karch, R., Knapp, B. & Ilieva, N. Relaxation estimation of rmsd in molecular dynamics immunosimulations. *Comput. Math. Method Med.* **2012**, 173521 (2012).
36. Khan, R. J. et al. Targeting SARS-CoV-2: A systematic drug repurposing approach to identify promising inhibitors against 3C-Like proteinase and 2'-O-Ribose Methyltransferase. *J. Biomol. Struct. Dyn.* **39**, 2679–2692 (2021).
37. Khan, S. A., Zia, K., Ashraf, S., Uddin, R. & Ul-Haq, Z. Identification of chymotrypsin-like protease inhibitors of SARS-CoV-2 via integrated computational approach. *J. Biomol. Struct. Dyn.* **39**, 2607–2616 (2021).
38. Pirolli, D. et al. Insights from molecular dynamics simulations: Structural basis for the V567D mutation-induced instability of zebrafish alpha-dystroglycan and comparison with the murine model. *PLoS ONE* **9**, e103866 (2014).
39. Bhardwaj, V. K. et al. Identification of bioactive molecules from tea plant as SARS-CoV-2 main protease inhibitors. *J. Biomol. Struct. Dyn.* **39**, 3449–3458 (2021).
40. Mishra, C. B. et al. Identifying the natural polyphenol catechin as a multi-targeted agent against SARS-CoV-2 for the plausible therapy of COVID-19: An integrated computational approach. *Brief. Bioinform.* **22**, 1346–1360 (2021).
41. Xu, Y. & Wang, R. A Computational Analysis of the Binding Affinities of FKBP12 Inhibitors Using the MM-PB/SA Method. *Proteins* **64**, 1058–1068 (2006).
42. Ossman, T., Fabre, G. & Trouillas, P. Interaction of Wine Anthocyanin Derivatives with Lipid Bilayer Membranes. *Comput. Theor. Chem.* **1077**, 80–86 (2016).
43. Lacey, D. L. et al. Osteoprotegerin Ligand Modulates Murine Osteoclast Survival in Vitro and in Vivo. *Am. J. Pathol.* **157**, 435–448 (2000).
44. Lacey, D. L. et al. Osteoprotegerin ligand is a cytokine that regulates osteoclast differentiation and activation. *Cell* **93**, 165–176 (1998).
45. Zhao, Y. et al. Conformational preferences of Pi-Pi stacking between ligand and protein, analysis derived from crystal structure data geometric preference of Pi-Pi interaction. *Interdiscip. Sci.* **7**, 211–220 (2015).

46. Seo, M., Park, J., Kim, E., Hohng, S. & Kim, H. Protein conformational dynamics dictate the binding affinity for a ligand. *Nat. Commun.* **5**, 3724 (2014).
47. Jiang, Y. et al. Identification of novel RANKL inhibitors through in silico analysis. *Bioorganic Chem.* **153**, 107826 (2024).
48. Li, J. et al. Inhibition of osteoclastogenesis and bone resorption in vitro and in vivo by a prenylflavonoid xanthohumol from hops. *Sci. Rep.* **5**, 17605 (2015).
49. Lee, J. et al. Inhibitory effect of luteolin on osteoclast differentiation and function. *Cytotechnology* **61**, 125–134 (2009).
50. Zhang, D., Zhang, J., Fong, C., Yao, X. & Yang, M. Herba epimedii flavonoids suppress osteoclastic differentiation and bone resorption by inducing G2 / M arrest and apoptosis. *Biochimie* **94**, 2514–2522 (2012).
51. Xiong, G. et al. ADMETlab 2.0: An integrated online platform for accurate and comprehensive predictions of ADMET properties. *Nucleic. Acids. Res.* **49**, W5–W14 (2021).
52. Daia, Y., Liaob, L. & Lic, D. On restart procedures for the conjugate gradient method. *Numer. Algorithms.* **35**, 249–260 (2004).
53. Laskowski, R. A., MacArthur, M. W., Moss, D. S. & Thornton, J. M. PROCHECK: A program to check the stereochemical quality of protein structures. *J. Appl. Crystallogr.* **26**, 283–291 (1993).
54. Hsin, K., Ghosh, S. & Kitano, H. Combining machine learning systems and multiple docking simulation packages to improve docking prediction reliability for network pharmacology. *PLoS ONE* **8**, e83922 (2013).
55. Lilkova, E. et al. The PyMOL Molecular Graphics System, Version 2.4 Schrodinger, LLC., 2015.
56. BIOVIA. Discovery Studio Visualizer, Version 2021.: Dassault Systèmes, 2021.
57. Purohit, R. Role of ELA region in auto-activation of mutant kit receptor: a molecular dynamics simulation insight. *J. Biomol. Struct. Dyn.* **32**, 1033–1046 (2014).
58. Nakashima, T. et al. Evidence for osteocyte regulation of bone homeostasis through rankl expression. *Nat. Med.* **17**, 1231–1234 (2011).
59. Malde, A. K. et al. An automated force field topology builder (atb) and repository: Version 1.0. *J. Chem. Theory Comput.* **7**, 4026–4037 (2011).
60. Abraham, M. J. et al. GROMACS: High performance molecular simulations through multi-level parallelism from laptops to supercomputers. *SoftwareX.* **1**, 19–25 (2015).
61. Schmid, N. et al. Definition and testing of the GROMOS force-field versions 54a7 and 54B7. *Eur. Biophys. J.* **40**, 843–856 (2011).
62. Darden, T., York, D. & Pedersen, L. Particle mesh ewald: An N?Log(N) method for ewald sums in large systems. *J. Chem. Phys.* **98**, 10089–10089 (1993).
63. Raniolo, S. & Limongelli, V. Ligand binding free-energy calculations with funnel metadynamics. *Nat. Protoc.* **15**, 2837–2866 (2020).
64. Kumari, R., Kumar, R. & Lynn, A. G_Mmpbsa–A GROMACS tool for high-throughput MM-PBSA calculations. *J. Chem Inf. Model.* **54**, 1951–1962 (2014).

Author contributions

Conceptualization, X.F.Z. and L.X.Z.; methodology, X.F.Z., D.L. and Q.W.; software,L.X.Z., L.B.W. and Z.Q.Z.; investigation, Q.W.; resources, L.X.Z. and Z.Q.Z.; data curation, D.L.; writing—original draft preparation, X.F.Z.; writing—review and editing, L.X.Z.; visualization, D.L.and L.B.W.; supervision, Z.Q.Z. and Y.X.; project administration, Y.X.; funding acquisition, Y.X. All authors have read and agreed to the published version of the manuscript.

Declarations

Competing interests

The authors declare no competing interests.

Additional information

Correspondence and requests for materials should be addressed to Y.X.

Reprints and permissions information is available at www.nature.com/reprints.

Publisher's note Springer Nature remains neutral with regard to jurisdictional claims in published maps and institutional affiliations.